# Theoretical and Experimental Studies of Compression and Shear Deformation Behavior of Osmium to 280 GPa

Chia-Min Lin, Kaleb Burrage, Chris Perreault, Wei-Chih Chen,
Cheng-Chien Chen*, and Yogesh K. Vohra*

*Department of Physics, University of Alabama at Birmingham, Birmingham, AL, 35294, USA*

E-mail: chencc@uab.edu; ykvohra@uab.edu

## Abstract

The compression behavior of osmium metal was investigated up to 280 GPa (volume compression $V/V_o$ =0.725) under nonhydrostatic conditions at ambient temperature using angle dispersive axial x-ray diffraction (A-XRD) with a diamond anvil cell (DAC). In addition, shear strength of osmium was measured to 170 GPa using radial x-ray diffraction (R-XRD) technique in DAC. Both diffraction techniques in DAC employed platinum as an internal pressure standard. Density functional theory (DFT) calculations were also performed, and the computed lattice parameters and volumes under compression are in good agreement with the experiments. DFT predicts a monotonous increase in axial ratio (*c/a*) with pressure and the structural anomalies of less than 1 % in (*c/a*) ratio reported below 150 GPa were not reproduced in theoretical calculations and hydrostatic measurements. The measured value of shear strength of osmium ($\tau$) approaches a limiting value of 6 GPa above a pressure of 50 GPa in contrast to theoretical predictions of 24 GPa and is likely due to imperfections in polycrystalline samples. DFT calculations also enable the studies of shear and tensile deformations. The theoretical ideal shear stress is found along the (001)[1-10] shear direction with the maximal shear stress ~24 GPa at critical strain ~0.13.

Keywords: osmium, incompressible materials, diamond anvil cell, compression and deformation behavior, lattice anomalies, density functional theory, ideal shear strength

## 1. Introduction

The fundamental understanding of behavior of materials under extreme conditions and search for materials with desirable mechanical properties like high shear strength are important endeavors in materials science. The most incompressible transition metal osmium has received extensive attention due to its high bulk modulus (incompressible nature), high shear modulus (resistance to deformation), and structural anomalies that have manifested themselves as anisotropic compression and have been attributed to changes in electronic structure under compression [1-5]. There are disagreements, however, into the location and existence of these structural anomalies in the hexagonal lattice c/a ratio. Dubrovinsky et al (2015) has reported osmium equation of state to 750 GPa where dips in c/a occurred at 150 GPa and 440 GPa respectively. These anomalies did not manifest themselves into the volumetric compression curve as it showed a monotonic decrease with pressure and were attributed to be topological changes in the Fermi surface (at 150 GPa) and electronic transitions for the higher-pressure region (at 440

GPa) [2]. Kenichi et al. (2004) reported a monotonic increase in c/a under quasi-hydrostatic conditions while results from Occelli et al. (2004) showed a change in slope of c/a around 25 GPa. More recent non-hydrostatic DAC compression to 207 GPa by Perreault et al. (2017) showed a broad minimum in c/a centralized at 75 GPa before a monotonic increase to the maximum pressure. Such disagreements warrant questions into the behavior of osmium lattice compression in relation to the degree of hydrostatic environment present in the DAC. Meanwhile, there are unresolved issues both in experiment and in the fundamental understanding of osmium under extreme conditions. The experimental uncertainty remains in achieving "true hydrostatic compression" conditions in the laboratory and measurement of axial ($c/a$) ratio under hydrostatic conditions and comparing the results with those obtained under "non-hydrostatic compression". In addition, experimentally, there is always an issue of hardness or resistance to plastic deformation of osmium under high pressure, and a direct measurement of shear strength under high pressures is highly desirable. The challenge on the theoretical calculations is to investigate the compression and deformation behavior and relate it to electronic structure changes including electron transfer from the s-band to d-band under compression [6], and changes in the topology of Fermi surface at high pressures that may give rise to anomalies in the axial ($c/a$) ratio. It has been suggested that the anomaly in c/a ratio can be attributed to non-hydrostatic and preferred orientation or texturing in polycrystalline osmium under high pressures [7]. Our motivation for the present work is to perform hydrostatic pressure measurement via radial x-ray diffraction study in a diamond anvil cell and experimentally demonstrate the presence or lack of anomaly in (c/a) ratio under true hydrostatic strain conditions in osmium.

Ideal strength is an important material property, defined as the stress required to permanently deform a perfect material (without defects). The critical shear stress that makes the perfect lattice unstable provides an assessment of the theoretical upper limit of material strength under large deformation strain. The radial x-ray diffraction technique in DAC provides an important opportunity in this study to measure shear strength of osmium metal under high pressures for comparison with theoretical calculations. In addition, we extend our non-hydrostatic measurements on osmium to 280 GPa, and the hydrostatic measurement to 170 GPa. Density functional theory (DFT) calculations still have great challenges in some respects, such as calculating dislocations and cracks under large indentation loads. Nevertheless, the DFT calculation accurately shows the plastic deformation mode and the stress-strain relationship of the crystal, which is of great significance for understanding the fracture mechanism of the crystal under plastic deformation. Several studies have used theoretical methods to investigate the incompressible nature of osmium, but the shear deformation is seldomly investigated. Here, we perform *ab initio* calculations on the shear deformation of osmium, obtaining its first theoretical strain-stress relation. Our work on fundamental compression and deformation behavior of osmium is thereby important for application under extreme conditions and for exploration and design of ultra-incompressible materials.

## 2. Experimental and Computational Methods

Angle dispersive axial x-ray diffraction (A-XRD) was performed on the osmium and platinum mixture at the Advanced Photon Source (APS) using HPCAT beamline 16-ID-B. The x-

ray beam size was 1 μm x 2 μm and the wavelength was 0.4066 Angstroms (30.5 KeV). Diffraction patterns were collected using a Pilatus 1M area CCD detector. Pressure was applied using a gas membrane and the sample to detector distance was calibrated using a NIST $CeO_2$ standard. Platinum powder (Alpha Aesar 99.97 % purity) was mixed with the osmium sample (Alpha Aesar 99.95 % purity) in a 1:3 volumetric ratio and used for sample pressure calibration up to 280 GPa. Compression to 280 GPa was conducted using a diamond anvil cell (DAC) apparatus utilizing toroidal diamond anvil technology. The culets of two 30-micron beveled diamond anvils were machined using a TESCAN LYRA 3 Focused Ion Beam to a culet diameter of 16 microns. A toroidal groove was machined around the culet to a depth of 3-5 microns and an outer diameter of 60 microns. The toroidal design helps prevent sample outflow under compression as well as supporting the diamond anvil from undergoing large deformation that leads to premature failure. For sample placement, a steel gasket was indented to a thickness of 30 microns and laser drilled with a sample hole of 8 microns. Osmium sample powder (Alpha Aesar 99.95 % purity) was packed into the sample hole mixed with platinum powder (Alpha Aesar 99.97 % purity) in a 1:3 volumetric ratio for pressure calibration.

For shear strength and estimation of experimental hydrostatic compression values, radial x-ray diffraction (R-XRD) at Beamline 16 BM-D, Advanced Photon Source, Argonne National Laboratory was conducted using beam energy of 30 keV and beam size 3.4 $\mu m$ vertical × 4.4 $\mu m$ horizontal at FWHM. A Double Multilayer Monochromator (DMM) was used to collimate the pink x-ray beam of $\lambda = 0.4133$ Å. Pink x-ray beams allow for shorter x-ray diffraction exposure time due to increased photon flux as high as 50 times that of previous collimators at Beamline 16 BM-D. Sample diffraction patterns were then collected on a MAR345 Image Plate with sample to detector distance of 286 mm calibrated using $CeO_2$ x-ray standard. A description of the R-XRD setup can be found in Ref. [8]. Sample compression for R-XRD experiments to 170 GPa was achieved using a panoramic Diamond Anvil Cell (DAC) with 70-micron beveled diamond anvils. The osmium and platinum sample were packed into a 25-micron sample hole in a Be gasket using the same volumetric ratio from the toroidal diamond anvil cell experiment. Both A-XRD and R-XRD experiments used bulk modulus values for platinum $B_0 = 276.4$ GPa $B_0' = 5.12$ [9] employed in the 3rd order Birch Murnaghan equation of state (BM EoS).

Collected radial x-ray diffraction patterns were integrated in 72 azimuthal segments of $\delta = 5$ degrees around the entire pattern using MAUD X-ray diffraction analysis software [10]. The measured d-spacing ($d_m$) of osmium sample for each 5-degree segment can be obtained using equation (1)[11]:

$$d_m(hkl) = d_p + d_p Q_{hkl}(1 - 3\cos^2\chi) \quad (1)$$

where $d_p$ is the hydrostatic component of compression, $Q_{hkl}$ is the lattice strain, and $\chi$ is the angle between the DAC compression axis and the diffraction plane normal defined by $cos\chi = cos\delta\, cos\theta$. The linear relationship between measured d-spacing $d_m$ and the $1 - 3\cos^2\chi$ term allows for direct calculation of the estimated hydrostatic d-spacing $d_p$ by eliminating the directionally dependent lattice strain $Q_{hkl}$ term when $1 - 3\cos^2\chi = 0$. When lattice strain $Q_{hkl}$ is present in a sample, the differential stress $t$ and shear strength $\tau$ can be determined by averaging the strain over all $hkl$ and using equation (2):

$$6 < Q_{hkl} > = \frac{t}{G}, t = 2\tau, \quad (2)$$

where $G$ is the sample shear modulus.

In our electronic and structural calculations, plane-wave pseudopotential density functional theory (DFT) [10, 11] calculation is performed using the projector augmented wave (PAW) method [12, 13] as implemented in VASP (the Vienna ab initio simulation package, version 5.4.4) [14, 15]. Perdew–Burke–Ernzerhof generalized gradient approximation (GGA-PBE) [16] is utilized for the exchange and correlation functional. The plane wave cut-off energy is set to 680 eV, and a Γ-centered Monkhors-Pack highly dense grid of 33 × 33 × 21 (resolution = 0.01 × 2π/Å) mesh is used for the Brillouin zone integration. The structure relaxation convergence criterion of atomic force is set to $10^{-3}$ eV/Å, and the self-consistent convergence criterion of the total energy is set to $10^{-7}$ eV/unit cell. A hexagonal primitive cell of osmium (space group P63/mmc) is used.

VASP allows the use of strain–stress method [14, 15, 17] to calculated elastic constant. The converged elastic constant can be obtained from the stress-strain relationship by imposing six finite deformations on the optimized crystal lattice [17, 18]. Within this strain–stress method, the final elastic constants are determined by the contributions of rigid ion deformation and ion relaxation. After computing the elastic constants, the bulk and shear moduli of the system are determined by using the Voigt–Reuss–Hill approximation [19-21].

To compute the shear and tensile strengths, we use the QE (Quantum ESPRESSO, version 6.3) DFT code [22-24], also with the PAW and GGA-PBE methods. We first calculate the optimal equilibrium structure at zero pressure and zero temperature by fully relaxing the crystal structure. The calculation setup and convergence criteria are the same as those used in the VASP calculations. After structure optimization, we calculate the shear deformation on various planes along different directions. Figure 1 shows an example of shear deformation on the (001) plane along the [1-10] direction with different strain values, using a 2×2×2 supercell with a momentum grid of 5 × 5 × 9 k-points. In each step of the shear deformation calculation, we fix the lattice constant and atomic positions of the axis perpendicular to the shear plane (*a* axis in Figure 1), and completely relax the lattice constants and atomic positions of the other two axes parallel to the shear plane (*b* and *c* axes in Figure 1). The tensile strength is also calculated in a similar way with tensile strain applied along the [001], [100] and [011] directions, using the 2×2×2 supercell with a momentum grid of 15 × 15 × 9 k-points.

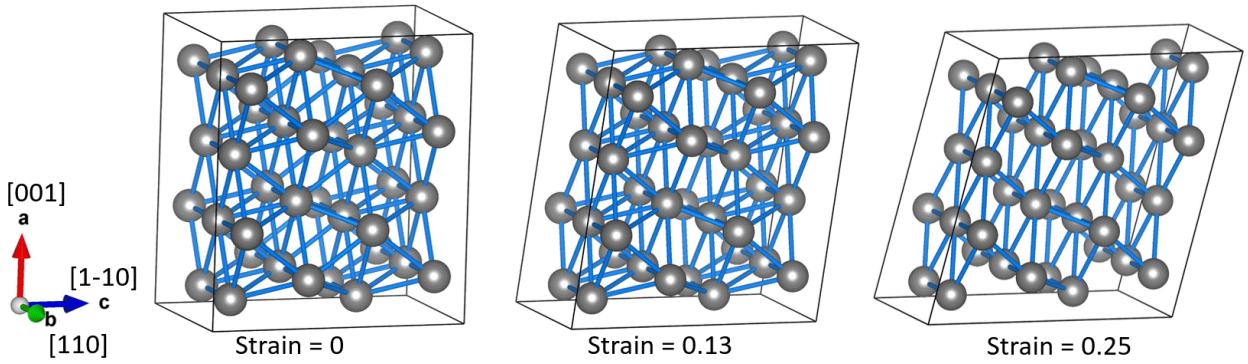


**Figure 1:** Shear deformation of osmium along the (001)[1-10] shear direction with strain values of 0, 0.13,

and 0.25, respectively. For neighboring atoms within 2.8 Å, they are connected by blue bonds. The VESTA software (version 3.4.8) is utilized to visualize the crystal structures [25].

## 3. Results

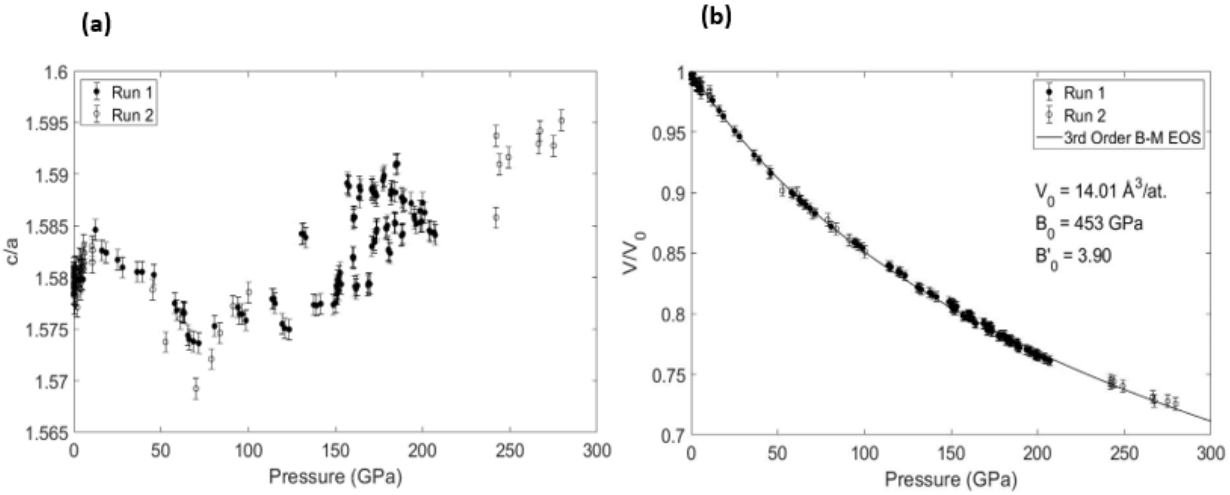


**Figure 2:** (a) The measured value of axial ratio (*c/a*) for the hexagonal close packed osmium for two non-hydrostatic experiments to 280 GPa. (b) The measured equation of state of osmium to 280 GPa along with the fit to the data.

Figure 2 displays the non-hydrostatic compression data for osmium *c*/*a* ratio for two experimental runs to 207 GPa (Run 1 [5]) and 280 GPa (Run 2), respectively. Both experimental runs revealed an anomaly between 50-70 GPa where *c*/*a* dropped from ~1.58 to ~1.57 before increasing linearly to the maximum pressure. Figure 2(b) plots the non-hydrostatic pressure-volume curve for each run to the maximum pressure with an overall volume compression of $V/V_0$ = 0.725 at 280 GPa. Non-hydrostatic equation of state fit to equation (1) results in a bulk modulus and its pressure derivative to be $B_0$ = 453 GPa and $B_0'$ = 3.90.

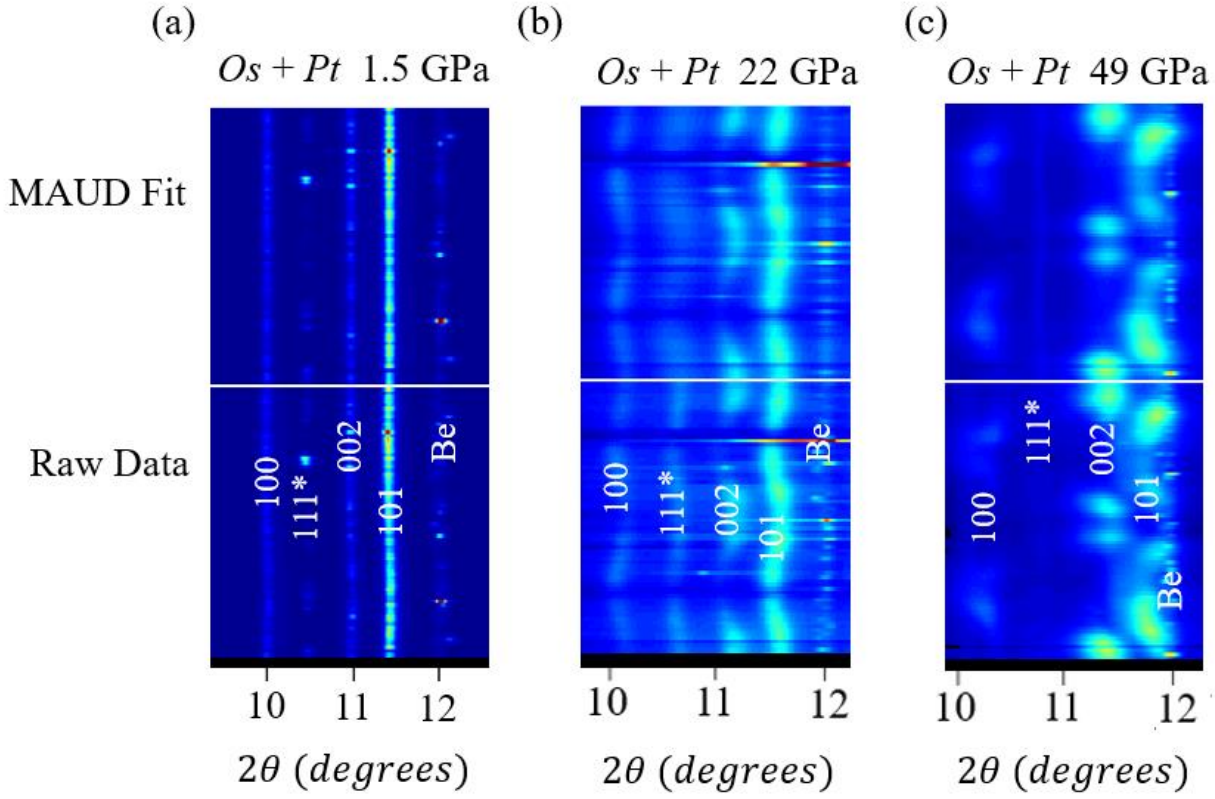


**Figure 3:** (a) Radial x-ray diffraction profile of Os-Pt mixture at 1.5 GPa corresponding to shear strength $\tau \sim 0.9\ GPa$ with labeled *hkl* values. (b) Radial x-ray diffraction profile of Os-Pt mixture at a pressure of 22 GPa. (c) Radial x-ray diffraction profile of Os-Pt mixture at a pressure of 49 GPa corresponding to flattening of shear strength at $\tau \sim 6\ GPa$ . Peaks labeled with asterisk (*) represent platinum pressure marker. Diffraction lines on the bottom half represent integrated raw data files while those on top are Rietveld refined using MAUD.

Stress induced effects on osmium sample can be seen by comparing different R-XRD diffraction patterns in Figure 3. Figure 3(a) presents x-ray diffraction pattern of Os-Pt sample at 0.8 GPa. The linearity of R-XRD *hkl* patterns in Figure 3(a) indicates diminutive shear effects present in the sample lattice structure. As internal stress and shear effects become prominent, the R-XRD *hkl* patterns display a curved profile as sample d-spacings are distorted maximally at $\delta = 0$ . This can be most clearly seen in Figure 3(c) when the Os-Pt mixture is at 49 GPa.

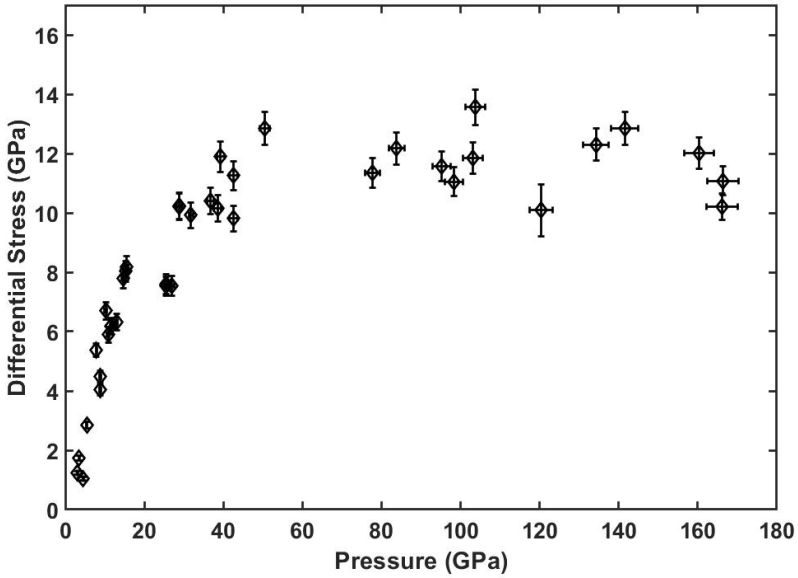


**Figure 4:** Measured value of the differential stress ($t$) using the shear modulus ($G$) calculated from DFT.

The lattice strain $Q_{hkl}$ is then averaged from the (100), (002), (101), and (102) hkl peaks and used in equation (2) to determine the differential stress. This is plotted in Figure 4 with the hydrostatic pressure values from platinum. The differential stress builds quickly between 0-40 GPa before plateauing at ~$t$= 12 GPa. Thus, the measured value of the shear strength for osmium is approximated to $\tau \sim 6\ GPa$

We next shift to our calculated results of osmium under hydrostatic pressure up to 300 GPa. The DFT-GGA estimated values of the lattice constant, volume, shear, and bulk moduli at ambient conditions are $a_0$ = 2.755 Å, $c_0$ = 4.345 Å, $V_0$ = 14.28 Å$^3$/atom, $G_0$ = 264 GPa, and $B_0$ = 406 GPa, respectively. The bulk moduli from different groups vary between 382 GPa to 476 GPa. In general, our calculation is consistent with the current experiment and other experimental and theoretical data reported previously [1-4, 26-28].

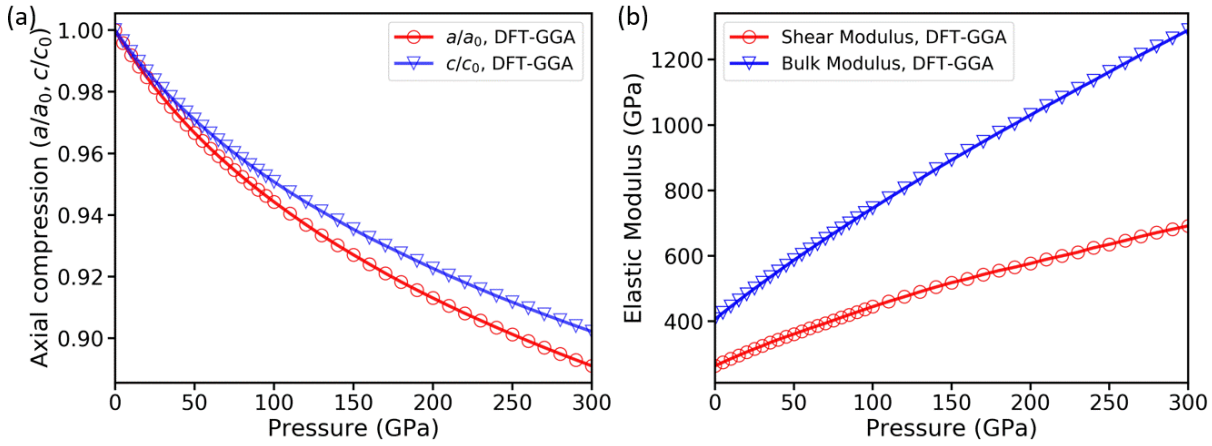


Figure 5. Theoretical results based on density functional theory (DFT) with a generalized gradient approximation (GGA) functional. (a) Axial compression of lattice parameters $a/a_0$ and $c/c_0$ versus pressure up to 300 GPa for osmium. (b) Bulk and Shear moduli as a function of pressure.

Figure 5(a) shows our theoretical results of hydrostatic pressure dependance of the axial compression lattice parameters $a/a_0$ and $c/c_0$ up to 300 GPa. The material exhibits anisotropic compression behavior and stability under high pressure. Compared with the experiments, the ambient lattice parameters $a_0 = 2.755$ Å and $c_0 = 4.345$ Å are within the error margin of 1%. Figure 5(b) displays the bulk and shear moduli as a function of pressure. The high bulk and shear moduli under compression demonstrate high incompressibility and deformation resistance of osmium.

The computed lattice parameter ratio *c/a* as a function of pressure is plotted in Figure 6(a) along with the experimental data, including the hydrostatic experiment. The theoretical *c/a* ratio does not show any obvious anomaly below 70 GPa. On the other hand, apart from the abnormalities, the overall theoretical trend of an increasing *c/a* ratio with pressure is the same as the experiment. Figure 6(b) shows the calculated volume compression $V/V_0$ under pressure along with the experimental data. The calculations are in excellent agreement with the experiments on the overall compression of $V/V_o = 0.725$ achieved in osmium at 280 GPa.

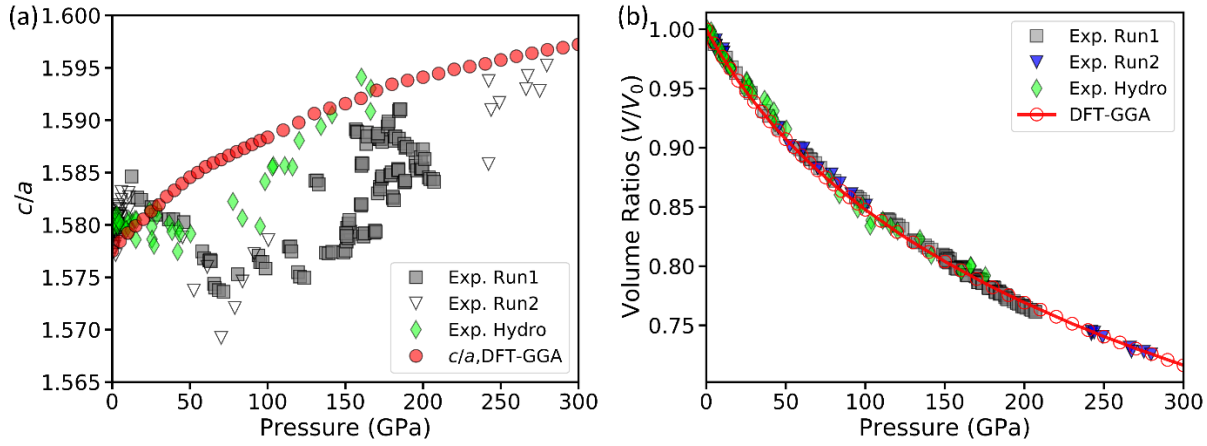


**Figure 6:** Pressure dependences of (a) lattice parameter *c/a* ratio, and (b) fractional unit cell volume curve up to 300 GPa for osmium, calculated by DFT-GGA plotted together with the experimental data obtained from two non-hydrostatic and one hydrostatic experiment.

Figure 7 presents the ideal strength calculations for shear and tensile stresses applied along difference directions. The stress versus strain curve increases linearly under small strains, and it exhibits a nonlinear behavior under large strains. The ideal stress value can be identified by the critical strain value where the stress begins to decrease. As seen in Figure 7(a), the ideal shear strength, i.e., the lowest peak shear stress in all directions, occurs on the (001) plane along the [1-10] direction. The ideal shear stress is ~23.53 GPa at a critical strain value of 0.13. Figure 7(b) displays the calculated tensile stress as a function of strain along the [001], [100], and [110] directions. The ideal tensile strength occurs in the [110] direction, which is the weakest tensile deformation direction of osmium. Table I summarizes the calculated data of maximal tensile and shear stresses and their corresponding critical strain values.

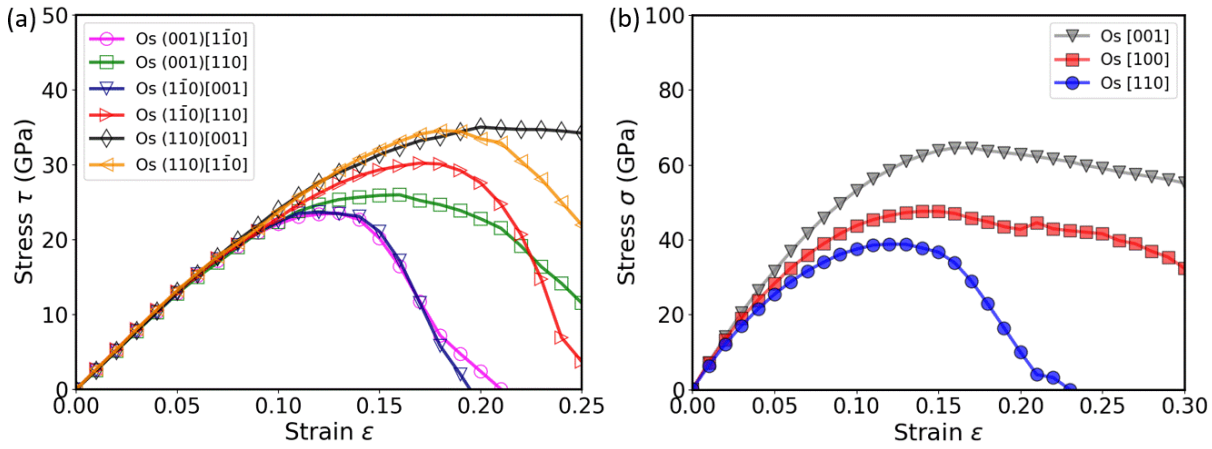


**Figure 7:** Stress-strain curves of osmium under (a) shear deformation up to strain value of 0.25 along various directions, (b) tensile deformation up to strain value of 0.30 in the [001], [100] and [110] directions. The results are based on DFT-GGA calculations.

| ***Osmium*** | | | | | | |
|---|---|---|---|---|---|---|
| ***Tensile deformation*** | | | | ***Shear deformation*** | | |
| | $\sigma_{max}$ | $\varepsilon_{max}$ | | | $\tau_{max}$ | $\varepsilon_{max}$ |
| [001] | 64.54 | 0.16 | | (001)[110] | 25.99 | 0.16 |
| [100] | 47.56 | 0.14 | | (001)[1-10] | 23.53 | 0.13 |
| [110] | 38.80 | 0.12 | | (110)[001] | 35.03 | 0.20 |
| | | | | (110)[1-10] | 34.57 | 0.18 |
| | | | | (1-10)[001] | 23.67 | 0.12 |
| | | | | (1-10)[110] | 30.21 | 0.17 |

Table I. [Left column] Peak stress $\sigma_{max}$ (in GPa) for tensile deformation and corresponding critical strain $\varepsilon_{max}$. [Right column] Peak stress $\tau_{max}$ (in GPa) for shear deformation and corresponding strain $\varepsilon_{max}$. The results are based on DFT-GGA calculations for osmium.

## 4. Discussion

The apparent dip in the *c*/*a* ratio between 50-70 GPa of about 1% [Figure 2(a)] causes further inquiry into whether the observed effect is induced by non-hydrostatic pressure environment, or if it is a physical phenomenon of the osmium crystal and electronic structure. Several experimental groups also have reported anomalies in the axial ratio *c*/*a* [4, 29, 30], which were attributed to an electronic topological transition (ETT) or known as a Lifshitz transition [31-35]. This type of transition occurs when the Fermi surface topology is altered by external perturbation. However, the simulated *c*/*a* ratios reported previously for osmium were inconsistent with the non-hydrostatic experimental observations [1, 3, 26-28, 30, 36]. Our DFT calculations also failed to observe anomalous *c*/*a* axial ratio upon non-hydrostatic compression. It needs to be emphasized that our calculations were performed at absolute zero temperature under hydrostatic pressure. Since the ETT effect causes the divergence of thermal expansion, the anomaly may not be visible at absolute zero temperature in theoretical calculations. It is also likely that (*c*/*a*) anomalies are due to non-hydrostatic strains in the crystal which are further enhanced due to any preferred orientations of the polycrystalline grains during compression. A combined DFT with

dynamical mean field theory (DMFT) [37] has been utilized to tackle quantum fluctuation effects in osmium, reporting the correlation between ETT and lattice anomalies. However, in that work [37], the lattice parameters were obtained directly from experimentally measured equation of state. Currently, it remains theoretically very challenging to fully relax crystal structures under pressure directly within DFT+DMFT approaches. Therefore, it is beyond the scope of our current research to address if lattice anomalies and ETT are concurring with strong electron interaction effects.

The DFT calculations also show high bulk modulus, high linear stiffness, and anisotropic compression of osmium, which can be attributed to its high valence electron density and strong directional bonding in the electronic structure. However, high bulk modulus does not guarantee a high resistant ability against large plastic deformation. Therefore, we can learn more about the mechanical properties in the deformation from the ideal shear and tensile stress-strain relationships. The ideal shear strength is the minimum value obtained in all possible shear directions at a certain critical strain, where the structure becomes unstable under deformation [38,39]. Our calculations show that the ideal shear strength of osmium occurs along the (001)[1-10] direction, with a peak shear stress value $\tau \sim 23.5$ GPa at critical strain $\varepsilon \sim 0.13$. The ideal strength of a material is related to the bonding in a crystal [40-42]. As seen in Figure 1, where atoms within 2.8 Å are connected by blue bonds, some bonds between osmium atoms are broken when the stress reached the critical strain along the (001)[1-10] direction.

Based on the Frenkel model [43], which uses a sinusoidal stress-strain relationship, the shear stress $\tau$ can be written as

$$\tau = \frac{Ga}{2\pi h} sin \frac{2\pi x}{a} \quad (9)$$

where $G$ is the shear modulus, $a$ is spacing between atoms in the direction of shear stress, $h$ is spacing of the rows of atoms, and $x$ is shear translation. When $sin \frac{2\pi x}{a} = 1$, we can obtain the maximal shear stress value $\tau_{max}$. Since $h \approx a$, we have

$$\tau_{max} \sim \frac{G}{2\pi} \sim \frac{G}{6} \quad (10)$$

When more refined models are used, the estimated maximal shear stress can vary from $\tau_{max} \approx G/10$ to $G/30$. In our DFT calculations, $\tau_{max}/G = 23.67/263.66 \approx 0.09$. The experimental shear stress value, however, is much smaller than the theoretical one, potentially due to defects and imperfections in real crystals, which reduce the mechanical strength of materials.

Finally, we discuss the relation between shear $\tau$ and tensile strength $\sigma$. Our shear strength results would suggest that the weakness tensile strength is along the [110] direction. Based on the relationship $\sigma = \sqrt{3}\tau$ [44], the weakest tensile stress along the [110] direction is $\sigma = \sqrt{3} \times 23.67 = 40.9$ (GPa). This estimated value is consistent with our calculations in Figure 7(b), where the weakest tensile stress is along the [110] direction, with a peak tensile stress value equal to 38.8 GPa at critical strain value 0.12.

## 5. Conclusions

Experimentally determined non-hydrostatic and hydrostatic elastic properties of polycrystalline osmium sample were obtained using a combination of angular dispersive axial x-ray diffraction (A-XRD) and radial x-ray diffraction (R-XRD) techniques. Density functional theory (DFT) calculations were also performed, and the computed lattice parameters and volumes under compression are in excellent agreement with the experiments. DFT predicts a monotonous increase in axial ratio (*c/a*) with pressure and the reported structural anomalies of less than 1 % in (*c/a*) ratio below 150 GPa were not reproduced in theoretical calculations. The hydrostatic lattice parameter data obtained from R-XRD studies clearly indicate that anomalies in (c/a) ratio are not present in true hydrostatic strain conditions providing experimental confirmation of earlier suggestions that (c/a) anomalies are due to non-hydrostatic and texture effects [7]. The shear strength of osmium was measured up to 170 GPa and shown to plateau at a value of $\tau \sim 6\ GPa$ above 50 GPa. The DFT ideal strength calculations indicate that the weakest deformation direction is along the (001)[1-10] shear direction, with a maximal stress $\tau_{max}$~24 GPa, about 0.09 of the shear modulus *G*. The experimental shear stress of 6 GPa is much smaller and is likely due to imperfections in real crystals. Our comprehensive investigations of osmium under high pressure provide detailed information about compression and deformation behaviors, which are important for achieving fundamental understanding and for applications in extreme environments.

## Acknowledgment

This research is funded by the U.S. National Science Foundation (NSF) under Metals and Metallic Nanostructures program Grant No. DMR-1904164. Portions of this work were performed at HPCAT (Sector 16), Advanced Photon Source (APS), Argonne National Laboratory. HPCAT operations are supported by DOE-NNSA's Office of Experimental Sciences. The Advanced Photon Source is a U.S. Department of Energy (DOE) Office of Science User Facility operated for the DOE Office of Science by Argonne National Laboratory under Contract No. DE-AC02-06CH11357. The calculations were performed on the Frontera computing system at the Texas Advanced Computing Center. Frontera is made possible by NSF award OAC-1818253.

## References

1. Cynn, H., et al., *Osmium has the lowest experimentally determined compressibility.* Physical review letters, 2002. **88**(13): p. 135701.
2. Dubrovinsky, L., et al., *The most incompressible metal osmium at static pressures above 750 gigapascals.* Nature, 2015. **525**(7568): p. 226-229.
3. Kenichi, T., *Bulk modulus of osmium: high-pressure powder x-ray diffraction experiments under quasihydrostatic conditions.* Physical Review B, 2004. **70**(1): p. 012101.
4. Occelli, F., et al., *Experimental evidence for a high-pressure isostructural phase transition in osmium.* Physical review letters, 2004. **93**(9): p. 095502.
5. Perreault, C.S., N. Velisavljevic, and Y.K. Vohra, *High-pressure structural parameters and equation of state of osmium to 207 GPa.* Cogent Physics, 2017. **4**(1): p. 1376899.
6. Pettifor, D., *Theory of energy bands and related properties of 4d transition metals. I. Band parameters and their volume dependence.* Journal of Physics F: Metal Physics, 1977. **7**(4): p. 613.

7. Godwal, B. K., Yan, J., Clark, S. M., & Jeanloz, R., High-pressure behavior of osmium: An analog for iron In Earth's core. Journal of Applied Physics, 2021. 111(11), 112608.

8. Burrage, K.C., C.Y. Park, and Y.K. Vohra, *Shear Strength and Hydrostatic Compression of Rhenium Diboride under High Pressures.* Journal of Applied Physics 2021. 129, 205901.
9. Yokoo, M., et al., *Ultrahigh-pressure scales for gold and platinum at pressures up to 550 GPa.* Physical Review B, 2009. **80**(10): p. 104114.
10. Hohenberg, P. and W. Kohn, *Inhomogeneous electron gas.* Physical review, 1964. **136**(3B): p. B864.
11. Kohn, W. and L.J. Sham, *Self-consistent equations including exchange and correlation effects.* Physical review, 1965. **140**(4A): p. A1133.
12. Blöchl, P.E., *Projector augmented-wave method.* Physical review B, 1994. **50**(24): p. 17953.
13. Kresse, G. and D. Joubert, *From ultrasoft pseudopotentials to the projector augmented-wave method.* Physical review b, 1999. **59**(3): p. 1758.
14. Kresse, G. and J. Furthmüller, *Efficiency of ab-initio total energy calculations for metals and semiconductors using a plane-wave basis set.* Computational materials science, 1996. **6**(1): p. 15-50.
15. Kresse, G. and J. Furthmüller, *Efficient iterative schemes for ab initio total-energy calculations using a plane-wave basis set.* Physical review B, 1996. **54**(16): p. 11169.
16. Perdew, J.P., K. Burke, and M. Ernzerhof, *Generalized gradient approximation made simple.* Physical review letters, 1996. **77**(18): p. 3865.
17. Le Page, Y. and P. Saxe, *Symmetry-general least-squares extraction of elastic data for strained materials from ab initio calculations of stress.* Physical Review B, 2002. **65**(10): p. 104104.
18. Wu, X., D. Vanderbilt, and D. Hamann, *Systematic treatment of displacements, strains, and electric fields in density-functional perturbation theory.* Physical Review B, 2005. **72**(3): p. 035105.
19. Hill, R., *The elastic behaviour of a crystalline aggregate.* Proceedings of the Physical Society. Section A, 1952. **65**(5): p. 349.
20. Voigt, W., *Lehrbuch der Kristallphysik, Leipzig, Taubner*. 1928, Springer, Berlin, Germany.
21. Reuß, A., *Berechnung der fließgrenze von mischkristallen auf grund der plastizitätsbedingung für einkristalle.* ZAMM-Journal of Applied Mathematics and Mechanics/Zeitschrift für Angewandte Mathematik und Mechanik, 1929. **9**(1): p. 49-58.
22. Giannozzi, P., et al., *QUANTUM ESPRESSO: a modular and open-source software project for quantum simulations of materials.* Journal of physics: Condensed matter, 2009. **21**(39): p. 395502.
23. Giannozzi, P., et al., *Advanced capabilities for materials modelling with Quantum ESPRESSO.* Journal of Physics: Condensed Matter, 2017. **29**(46): p. 465901.
24. Giannozzi, P., et al., *Quantum ESPRESSO toward the exascale.* The Journal of chemical physics, 2020. **152**(15): p. 154105.
25. Momma, K. and F. Izumi, *VESTA 3 for three-dimensional visualization of crystal, volumetric and morphology data.* Journal of applied crystallography, 2011. **44**(6): p. 1272-1276.
26. Weinberger, M.B., S.H. Tolbert, and A. Kavner, *Osmium metal studied under high pressure and nonhydrostatic stress.* Physical review letters, 2008. **100**(4): p. 045506.
27. Armentrout, M.M. and A. Kavner, *Incompressibility of osmium metal at ultrahigh pressures and temperatures.* Journal of Applied Physics, 2010. **107**(9): p. 093528.
28. Godwal, B., et al., *High-pressure behavior of osmium: an analog for iron in Earth's core.* Journal of Applied Physics, 2012. **111**(11): p. 112608.

29. Sahu, B. and L. Kleinman, *Osmium is not harder than diamond.* Physical Review B, 2005. **72**(11): p. 113106.
30. Ma, Y., et al., *Electronic and crystal structures of osmium under high pressure.* Physical Review B, 2005. **72**(17): p. 174103.
31. Lifshitz, I., *High-pressure anomalies of electron properties of a metal.* Zh. Eksp. Teor. Fiz., 1960. **38**: p. 1569.
32. Efthimiopoulos, I., et al., *High-pressure studies of Bi2S3.* The Journal of Physical Chemistry A, 2014. **118**(9): p. 1713-1720.
33. Gomis, O., et al., *Lattice dynamics of Sb 2 Te 3 at high pressures.* Physical Review B, 2011. **84**(17): p. 174305.
34. Bruno, E., et al., *Fermi surfaces and electronic topological transitions in metallic solid solutions.* Physics Reports, 1994. **249**(6): p. 353-419.
35. Vilaplana, R., et al., *High-pressure vibrational and optical study of Bi 2 Te 3.* Physical Review B, 2011. **84**(10): p. 104112.
36. Pantea, C., et al., *Bulk modulus of osmium, 4–300 K.* Acta Materialia, 2009. **57**(2): p. 544-548.
37. Feng, Q., et al., *Topological transitions of the Fermi surface of osmium under pressure: an LDA+ DMFT study.* New Journal of Physics, 2017. **19**(3): p. 033020.
38. Ogata, S., et al. *Ab initio study of ideal shear strength*. in *IUTAM symposium on mesoscopic dynamics of fracture process and materials strength*. 2004. Springer.
39. Ogata, S., et al., *Ideal shear strain of metals and ceramics.* Physical Review B, 2004. **70**(10): p. 104104.
40. Yang, J., H. Sun, and C. Chen, *Is osmium diboride an ultra-hard material?* Journal of the American Chemical Society, 2008. **130**(23): p. 7200-7201.
41. Fan, T.-W., et al., *Ideal strength of Mg2X (X= Si, Ge, Sn and Pb) from first-principles.* Journal of Magnesium and Alloys, 2013. **1**(2): p. 163-168.
42. Zang, C., et al., *Indentation strength of ultraincompressible rhenium boride, carbide, and nitride from first-principles calculations.* Physical Review B, 2012. **86**(1): p. 014108.
43. Frenkel, J., *Zur theorie der elastizitätsgrenze und der festigkeit kristallinischer körper.* Zeitschrift für Physik, 1926. **37**(7-8): p. 572-609.
44. Mises, R.v., *Mechanik der festen Körper im plastisch-deformablen Zustand.* Nachrichten von der Gesellschaft der Wissenschaften zu Göttingen, Mathematisch-Physikalische Klasse, 1913: p. 582-592.